NUCLEAR MATTER APPROACH TO THE OPTICAL POTENTIAL FOR SCATTERING OF ^{16}O AND ^{40}Ca IONS*

By J. Dąbrowski

Institute for Nuclear Studies, Warsaw**

(Received August 1, 1988)

A simple theory of the heavy-ion optical potential $\mathscr{V} = \mathscr{V}_R + i\mathscr{V}_I$ is applied to ^{16}O and ^{40}Ca nuclei. The colliding ions are described locally as two slabs of nuclear matter with the frozen density model for the local density and momentum distribution. $\mathscr{V}_R$ is defined as the energy difference between overlapping and separated nuclei. The energy density of the two slabs is derived from the properties of nuclear matter, and supplemented by inhomogeneity corrections. For $\mathscr{V}_I$ the frivolous model is applied. $\mathscr{V}_R$ agrees with, and $\mathscr{V}_I$ is smaller than results of "exact" $\mathscr{K}$ matrix calculations.

PACS numbers: 25.70.-z

1. Introduction

In the present paper, the simple nuclear matter (NM) approach to the heavy-ion optical potential $\mathscr{V} = \mathscr{V}_R + i\mathscr{V}_I$ presented in [1] (hereafter referred to as I) is applied to ^{16}O and ^{40}Ca ions. In a simplified form, the approach was employed a long time ago by Brueckner et al. [2]. It is based on the local density approximation: the two colliding nuclei are described locally as two interpenetrating slabs of NM, moving against each other. For the local density and momentum distribution the frozen density model is applied. The real part $\mathscr{V}_R$ of $\mathscr{V}$ is defined as the difference between the energies of the overlapping and spatially separated nuclei. The difficult task of solving the two slab problem starting from the NN interaction is bypassed by a simpler procedure. The energy of the two slabs — and thus the real potential $\mathscr{V}_R$ — is determined directly from the known properties of NM. For the imaginary potential $\mathscr{V}_I$ the frivolous model is applied, and thus $\mathscr{V}_I$ is expressed directly through the NN cross section. Empirical density distributions, determined by electron scattering, are used for the colliding nuclei.

The paper is organized as follows. In Section 2, a short presentation of the local density approximation for $\mathscr{V}_R$ and $\mathscr{V}_I$ is given. In Section 3, the frozen density model

* Research partly supported by the Polish-U.S. Maria Skłodowska-Curie Found under Grant No P-F7F037P.

** Address: Instytut Problemów Jądrowych, Hoża 69, 00-681 Warszawa, Poland.

for the local density and momentum distribution in the system of two colliding nuclei is described. In Section 4, results for two slabs of NM are presented. In Section 5, the inhomogeneity corrections to the energy density are introduced. In Section 6, the calculational procedure is outlined. In Section 7, results obtained for ^{16}O and ^{40}Ca are presented and discussed. A summary and conclusions are given in Section 8.

2. *The local density approximation*

2.1. The real part of $\mathscr{V}$

We consider nuclei 1 and 2 (with masses M_1 and M_2) moving in the CMS with relative momentum $\boldsymbol{K}_{\mathrm{REL}}$ (in units of $\hbar$) and energy E (see Fig. 1). We denote by $\boldsymbol{R}$ the relative position vector between the centers of mass of 1 and 2. We define the real part of the optical potential $\mathscr{V}_{\mathrm{R}} = \mathscr{V}_{\mathrm{R}}(E, R)$ between the two nuclei by splitting the nuclear CM energy $\mathscr{E}_{\mathrm{CM}}(K_{\mathrm{REL}}, R)$ into the kinetic energy of the relative motion of nuclei 1 and 2, $\hbar^2 K_{\mathrm{REL}}^2/2\mu$ [$\mu = M_1 M_2/(M_1 + M_2)$], the intrinsic nuclear energies of isolated nuclei 1 and 2, $\mathscr{E}_{\mathrm{in}}(1)$, and $\mathscr{E}_{\mathrm{in}}(2)$, and $\mathscr{V}_{\mathrm{R}}$:

$$\mathscr{E}_{\mathrm{CM}}(K_{\mathrm{REL}}, R) = \hbar^2 K_{\mathrm{REL}}^2/2\mu + \mathscr{E}_{\mathrm{in}}(1) + \mathscr{E}_{\mathrm{in}}(2) + \mathscr{V}_{\mathrm{R}}(E, R). \tag{2.1}$$

During the collision, the instantaneous relative momentum is changing with R, $K_{\mathrm{REL}} = K_{\mathrm{REL}}(R)$, in such a way as to conserve the total energy:

$$\mathscr{E}_{\mathrm{CM}}(K_{\mathrm{REL}}(R), R) + \mathscr{V}_{\mathrm{C}}(R) = E, \tag{2.2}$$

where $\mathscr{V}_{\mathrm{C}}(R)$ is the Coulomb potential between nuclei 1 and 2. Energy conservation Eq. (2.2), which may be written as

$$\hbar^2 K_{\mathrm{REL}}(R)^2/2\mu + \mathscr{V}_{\mathrm{R}}(E, R) + \mathscr{V}_{\mathrm{C}}(R) = \hbar^2 K_{\mathrm{REL}}(\infty)^2/2\mu = E, \tag{2.3}$$

determines the dependence of K_{REL} on R.

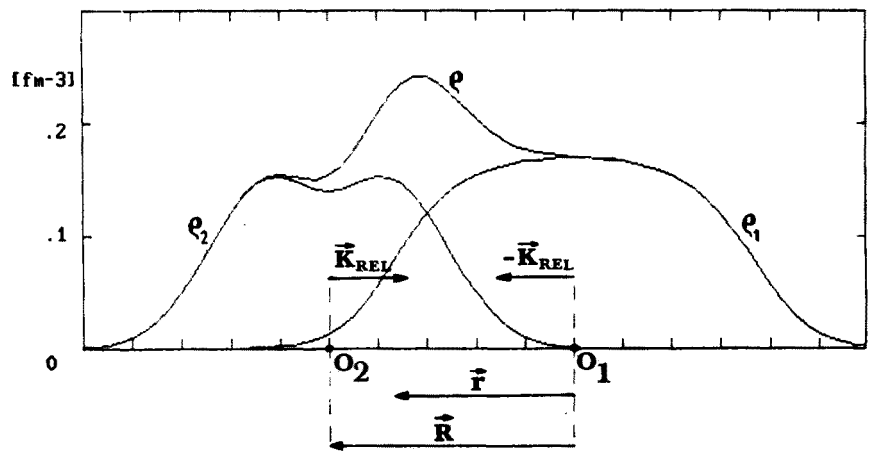

Fig. 1. The density distribution in two colliding nuclei. The CM of nucleus 1(2) is $0_1(0_2)$

We apply the energy density formalism, and write $\mathscr{E}_{CM}$ in the form

$$\mathscr{E}_{CM}(K_{REL}, R) = \int dr H_{CM}(K_{REL}, R; r), \tag{2.4}$$

where H_{CM} is the energy density (in CMS) at r. We assume that for a given distance R between the two nuclei, the system may be approximated locally (at each point r) by a piece of NM of total density ϱ and with momentum distribution $n(k_N)$. Obviously, we have

$$\varrho = [4/(2\pi)^3] \int dk_N n(k_N), \tag{2.5}$$

where the factor 4 takes care of the four spin-isospin states (we assume that both colliding nuclei are spin and isospin saturated).

At the moment, we do not consider the problem of determining ϱ and n, which we shall overcome later (in Sect. 3) with the frozen density model. Our present task is to determine the energy density H of NM with given ϱ and n. Instead of trying to do it starting from the NM interaction, we relate H to the properties of normal NM, i.e., NM in its ground state.

We consider normal NM of the same density ϱ as the local density of our system of colliding nuclei. In this normal NM, the momentum distribution is

$$n_0(k_N) = \theta(k_F - k_N), \tag{2.6}$$

where the Fermi momentum

$$k_F = (3\pi^2 \varrho/2)^{1/3}, \tag{2.7}$$

and the energy density is

$$H_0 = (E_{NM}/A)\varrho = f(\varrho)\varrho, \tag{2.8}$$

where $f(\varrho) = E_{NM}/A$ is the energy per nucleon in normal NM.

Expressions (2.6)–(2.8) are of course valid only in the rest frame of NM (in which the total momentum vanishes), which we shall call the local center of mass (cm) frame. From now on, we shall denote by k_N nucleon momenta, and by H the energy density of NM in this cm frame.

For the difference between H and H_0, we use the approximate relation

$$H - H_0 = H - f\varrho = [4/(2\pi)^3] \int dk_N [n(k_N) - n_0(k_N)] e_0(k_N) \tag{2.9}$$

(e_0 is the s.p. energy in normal NM), which is valid when the difference n-n_0 is small. [Neglected in (2.9) is the change in the effective two-body interaction induced by the change in the momentum distribution.]

For the s.p. energy e_0, we assume the effective mass approximation:

$$e_0(k_N) = \varepsilon(k_N) + V_0(k_N) = \varepsilon(k_N)/v + C, \tag{2.10}$$

where $\varepsilon(k_N) = \hbar^2 k_N^2/2m$, V_0 is the s.p. potential, and $v = m^*/m$ is the ratio of the effective to the real nucleon mass. Inserting (2.10) into (2.9) gives

$$H = f\varrho + (\tau - \tau_0)/v. \tag{2.11}$$

where τ and τ_0 are the kinetic energy densities (in the cm frame) in our system and in normal NM:

$$\tau = [4/(2\pi)^3] \int d\boldsymbol{k}_N n(\boldsymbol{k}_N)\varepsilon(k_N), \tag{2.12}$$

$$\tau_0 = [4/(2\pi)^3] \int d\boldsymbol{k}_N n_0(k_N)\varepsilon(k_N) = (3/5)\varepsilon(k_F)\varrho.$$

For the semi-empirical function $f(\varrho)$, we use the form:

$$f(\varrho) = (3/5)\varepsilon(k_F) + \sum_{I=3}^{5} a_I (k_F/k_{F0})^I, \tag{2.13}$$

where k_{F0} is the Fermi momentum at the equilibrium density ϱ_0, and the coefficients a_I are determined by k_{F0}, by the volume energy of NM, $\varepsilon_{vol} = f(\varrho_0)$, and by the compressibility $K_c = k_{F0}^2 (d^2 f/dk_F^2)_0$.

To fix the value of v, we notice that Eq. (2.10) implies that $dV_0/de_0 = 1 - v$. Since the empirical energy dependence of V_0 (i.e., of the depth of the real optical potential) is $dV_0/de_0 \cong 0.3$ (see p. 237 of [3]), we get $v_0 = v(\varrho_0) = 0.7$. For the dependence of v on ϱ, we use the form [4]

$$v = v(\varrho) = 1/[1 + (1/v_0 - 1)\varrho/\varrho_0]. \tag{2.14}$$

2.2. The imaginary part of $\mathscr{V}$

In the case of the nucleon-nucleus optical potential, one may express the imaginary part of the potential directly through the NN cross section. The procedure, known as the frivolous model, is extended here to the case of the nucleus-nucleus optical potential. In I, the frivolous model expression for $\mathscr{V}_I$ was derived from the equation for the effective NN interaction (the $\mathscr{K}$ matrix) by applying the optical theorem. Here, we restrict ourselves to an intuitive motivation of this expression.

The absorption in the nucleus-nucleus scattering is caused by NN collisions which carry the system out of the elastic channel. These collisions may take place in all volume elements, and thus

$$\mathscr{V}_I(E, R) = \int d\boldsymbol{r} v_I(K_{REL}, R; \boldsymbol{r}), \tag{2.15}$$

where the absorptive potential density v_I is the contribution to $\mathscr{V}_I$ of the NN collisions in the unit volume at $\boldsymbol{r}$. In our local density approximation, we consider the unit volume at $\boldsymbol{r}$ as a piece of NM of density ϱ and momentum distribution $n(\boldsymbol{k}_N)$. In this unit volume, the probability per unit time of a collision between a nucleon with an arbitrary momentum $\boldsymbol{k}_1$ and another nucleon with an arbitrary momentum $\boldsymbol{k}_2$ is

$$w_0 = (1/2)\,[4/(2\pi)^3]^2 \int d\boldsymbol{k}_1 n(\boldsymbol{k}_1) \int d\boldsymbol{k}_2 n(\boldsymbol{k}_2) v\sigma, \tag{2.16}$$

where σ is the total NN cross section, and $v = 2\hbar k/m$ is the relative velocity of the two nucleons, where k is their relative momentum,

$$\boldsymbol{k} = (\boldsymbol{k}_1 - \boldsymbol{k}_2)/2. \tag{2.17}$$

The factor 1/2 in (2.16) prevents double counting.

The most important many-body effect which has to be incorporated into semi-classical expression (2.16) is the Pauli blocking of the occupied final states in the NN scattering in NM. We denote the final momenta in the NN scattering by $\boldsymbol{k}_1'$ and $\boldsymbol{k}_2'$, and the final relative momentum by $\boldsymbol{k}' = (\boldsymbol{k}_1' - \boldsymbol{k}_2')/2$. Notice that the total momentum $2\boldsymbol{K} = \boldsymbol{k}_1 + \boldsymbol{k}_2 = \boldsymbol{k}_1' + \boldsymbol{k}_2'$ is conserved in the scattering. Let us write the total NN cross section σ in terms of the differential cross section: $\sigma = \int d\hat{\boldsymbol{k}}' d\sigma/d\hat{\boldsymbol{k}}'$. If the final state $\boldsymbol{k}_1'$ or $\boldsymbol{k}_2'$ is occupied by other nucleons of NM, the Pauli principle prevents the scattering into these states. To take it into account, we make the replacement:

$$\sigma \to \int d\hat{\boldsymbol{k}}' Q(\boldsymbol{K}, \boldsymbol{k}') d\sigma/d\hat{\boldsymbol{k}}' \cong \int d\hat{\boldsymbol{k}}' Q(\boldsymbol{K}, \boldsymbol{k}')\sigma/4\pi = \bar{Q}(\boldsymbol{K}, k)\sigma, \tag{2.18}$$

where the Pauli blocking operator

$$Q(\boldsymbol{K}, \boldsymbol{k}') = [1 - n(\boldsymbol{k}_1')][1 - n(\boldsymbol{k}_2')] = [1 - n(\boldsymbol{K} + \boldsymbol{k}')][1 - n(\boldsymbol{K} - \boldsymbol{k}')], \tag{2.19}$$

and the angle-averaged operator

$$\bar{Q}(\boldsymbol{K}, k) = (1/4\pi) \int d\hat{\boldsymbol{k}} Q(\boldsymbol{K}, \boldsymbol{k}). \tag{2.20}$$

In the first step in (2.18) we approximate $d\sigma/d\hat{\boldsymbol{k}}'$ by $\sigma/4\pi$, and in the second step we assume that $k' = k$.

Another important many-body effect is the dispersion, i.e., the momentum dependence of the s.p. potential [see Eq. (2.10)], which leads to the appearance of the factor $v = m^*/m$ in the expression for the collision probability. This may be easily understood because the probability is proportional to the density of final states (the number of momentum states per unit energy), which in turn is proportional to the effective mass. Of course, using for v the value determined in normal NM involves an approximation discussed in I.

Thus the Pauli blocking and dispersive effects modify expression (2.16) to

$$w = (1/2)v[4/(2\pi)^3]^2 \int d\boldsymbol{k}_1 n(\boldsymbol{k}_1) \int d\boldsymbol{k}_2 n(\boldsymbol{k}_2) \bar{Q}(\boldsymbol{K}, k)(2\hbar k/m)\sigma. \tag{2.21}$$

For the absorptive potential density v_I, connected with w by the relation $v_I = -\hbar w/2$, we get

$$v_I = -v(\hbar^2/2m)[4/(2\pi)^3]^2 \int d\boldsymbol{k}_1 n(\boldsymbol{k}_1) \int d\boldsymbol{k}_2 n(\boldsymbol{k}_2) \bar{Q}(\boldsymbol{K}, k) k\sigma(k). \tag{2.22}$$

3. The frozen density approximation

In this Section, we present a simple way of determining the local density ϱ and momentum distribution, known as the frozen density approximation. In this approximation all degrees of freedom are frozen, except for R. The density of each of the two nuclei does not relax during the collision. The instantaneous velocity of each point of the nucleus 1(2) is the same [in CMS it is equal $-\hbar \boldsymbol{K}_{\mathrm{REL}}/M_1$ $(\hbar \boldsymbol{K}_{\mathrm{REL}}/M_2)$].

The total local density of the combined system at $\boldsymbol{r}$ is equal to the sum of the original densities of nuclei 1 and 2 (see Fig. 1):

$$\varrho(\boldsymbol{r}) = \varrho_1(\boldsymbol{r}) + \varrho_2(|\boldsymbol{r} - \boldsymbol{R}|). \tag{3.1}$$

As far as the momentum distribution is concerned, it should be reminded that n is the momentum distribution in the noninteracting system (in particular, in normal NM it is represented by the Fermi sphere $n = n_0$).

In the rest frame of nucleus 1 (the frame with the origin in $\tilde{O}_1$ — see Fig. 2), the local momentum distribution at r of nucleons in nucleus 1 is the Fermi sphere (surface F_1) center in $\tilde{O}_1$, with the local Fermi momentum

$$k_{F10} = k_{F10}(r) = [3\pi^2 \varrho_1(r)/2]^{1/3}. \tag{3.2}$$

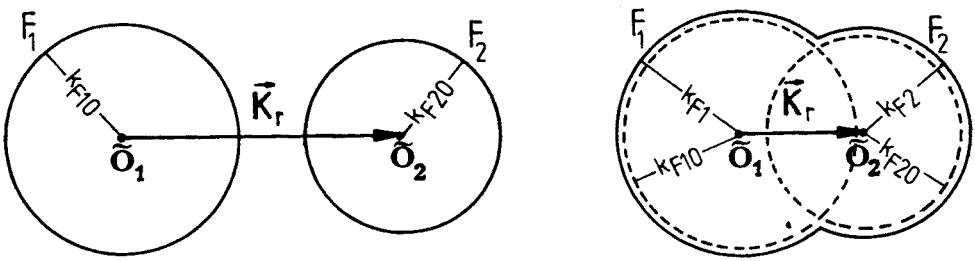

Fig. 2. The local momentum distribution in two colliding nuclei

In the rest frame of nucleus 1, nucleus 2 moves with velocity $\hbar \boldsymbol{K}_{REL}/\mu$, and at each point r the average momentum $\boldsymbol{K}_r$ of nucleons in nucleus 2 is

$$\boldsymbol{K}_r = (m/\mu)\boldsymbol{K}_{REL}. \tag{3.3}$$

Hence the local momentum distribution at r of nucleons in nucleus 2 is a Fermi sphere (surface F_2) centered in $\tilde{O}_2$ (with $\overrightarrow{\tilde{O}_1\tilde{O}_2} = \boldsymbol{K}_r$), with a local Fermi momentum (see Fig. 1)

$$k_{F20} = k_{F20}(r) = [3\pi^2 \varrho_2(|r-R|)/2]^{1/3}. \tag{3.4}$$

Of course, we may define $\boldsymbol{K}_r$ independently of any reference frame, as the difference between the average momenta of nucleons in nucleus 2 and of nucleons in nucleus 1. Thus we may call $\boldsymbol{K}_r$ (twice) the average relative NN momentum.

For the combined system of nuclei 1 and 2, we obtain the local momentum distribution n consisting of two Fermi spheres with surfaces F_1 and F_2: all s.p. momentum states within the Fermi surface $F = F_1 + F_2$ are occupied, and the states outside of F are empty.

The situation when $K_r > k_{F10}+k_{F20}$, shown in Fig. 2(a), presents no problem. If however $k_r < k_{F10}+k_{F20}$ [Fig. 2(b)], the two Fermi surfaces overlap, and the problem arises of a double occupancy within the overlap region. In resolving this problem, we apply the prescription of [5]: we increase both Fermi momenta k_{F10} and k_{F20} by the same amount δ,

$$k_{F1} = k_{F10}+\delta, \quad k_{F2} = k_{F20}+\delta, \tag{3.5}$$

and determine δ from condition (2.5) with ϱ given by Eq. (3.1):

$$\varrho = \varrho_1 + \varrho_2 = [4/(2\pi)^3]V_F, \tag{3.6}$$

where V_F is the volume within $F = F_1 + F_2$. In the extreme case when F_2 lies within F_1 (or F_1 within F_2), i.e., when $K_r < |k_{F10} - k_{F20}|$, only one Fermi surface F_1 (or F_2) remains, with the radius equal to $[3\pi^2\varrho/2]^{1/3}$.

In conclusion, the frozen density approximation (plus the prescription to avoid a double occupancy) leads to the local density ϱ, Eq. (3.1), and to the two-sphere momentum distribution of Fig. 2 specified by the parameters K_r, $k_{F1}(r)$ and $k_{F2}(r)$, determined by K_{REL}, Eq. (3.3), and by $\varrho_1(r)$ and $\varrho_2(|r-R|)$, Eqs. (3.4)–(3.6).

With the two-sphere momentum distribution n, one may obtain analytical expressions for the kinetic energy density τ, Eq. (2.12), and for the angle-averaged Pauli blocking operator $\bar{Q}$, Eq. (2.20) [see Appendix in I].

4. Results for two slabs of NM

In all our calculations, we use the following parameters of normal NM: $k_{F0} = 1.35\ \text{fm}^{-1}$ ($\varrho_0 = 0.166\ \text{fm}^{-3}$), $\varepsilon_{vol} = -15.8$ MeV, $K_c = 235$ MeV, and $v_0 = .7$.

For the total NN cross section σ for the NN scattering with the laboratory energy $E_L > 20$ MeV, we use the parametrization [6]:

$$\sigma = (\sigma_{nn} + \sigma_{np})/2 = (2.2356/\beta^2 - 5.606/\beta + 6.255)\text{fm}^2, \tag{4.1}$$

where β is the relative NN velocity in units of c,

$$\beta = v/c = (2E_L/mc^2)^{1/2} = 2\hbar k/mc. \tag{4.2}$$

For $E_L < 20$ MeV, we use the effective range approximation with the following values (in fm) of the respective singlet (s) and triplet (t) scattering lengths (a) and effective ranges (r): $a_{snn} = -16.1$, $r_{snn} = 3.2$, $a_{snp} = -23.714$, $r_{snp} = 2.704$, $a_{tnp} = 5.4$, and $r_{tnp} = 1.73$.

We consider two slabs of equal density $\varrho_1 = \varrho_2 = \varrho/2$, moving against each other with relative velocity K_r/m. For the momentum distribution n, we assume the two-sphere distribution of Fig. 2. In this homogeneous system, the energy $\mathscr{E}_{CM} = H \times$(volum of the system) is infinite, and we introduce the energy per nucleon $\mathscr{E}_{CM}/A = H/\varrho$, and similarly $\mathscr{V}/A$, where A is the total number of nucleons in the two slabs. Notice that in the two slab system, the cm frame coincides with CMS, and $H_{CM} = H$. For the intrinsic energies, we have $\mathscr{E}_{in}(1)/(A/2) = \mathscr{E}_{in}(2)/(A/2) = f(\varrho/2)$.

In the homogeneous system of two slabs, K_r is constant [for two equal slabs $K_r = 4K_{REL}/A$ — see Eq. (3.3)], and we present in Fig. 3 our results for $\mathscr{V}/A$ as functions of K_r for the total density $\varrho = \varrho_0/2$ (A), $\varrho = \varrho_0$ (B), and $\varrho = 2\varrho_0$ (C).

The potential energy contribution to $\mathscr{V}_R/A$ increases with K_r (which may be traced back to the short range NN repulsion) and the kinetic energy contribution (the increase in the kinetic energy caused by the Pauli blocking when the two Fermi spheres overlap) decreases with K_r. The net result is the initial decrease in $\mathscr{V}_R/A$ and the appearance of

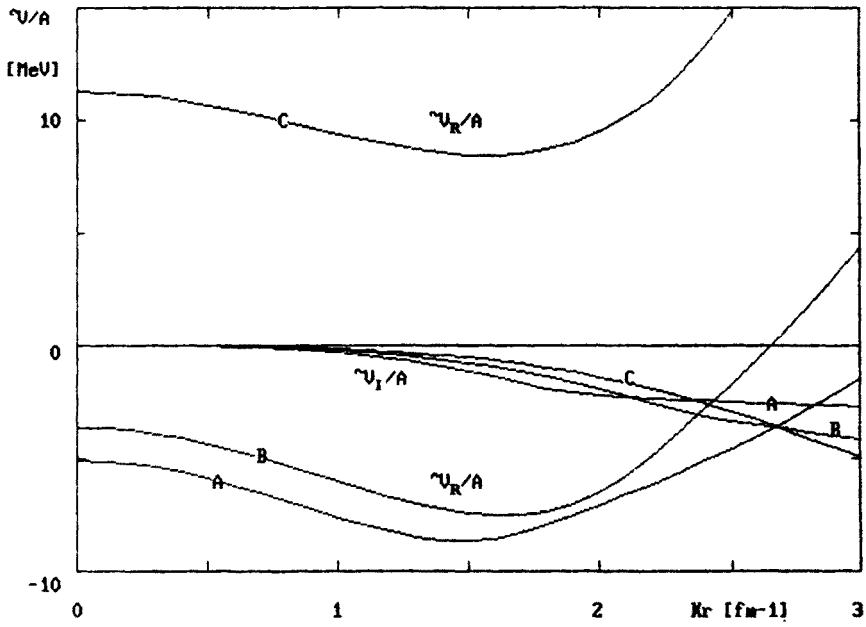

Fig. 3. $\mathscr{V}_R/A$ and $\mathscr{V}_I/A$ for two colliding slabs of NM of the same density as functions of K_r for the total density $\varrho = \varrho_0/2$ (A), $\varrho = \varrho_0$ (B), and $\varrho = 2\varrho_0$ (C)

a "window" of a minimum in $\mathscr{V}_R/A$ at $K_r \cong 1.5\,\mathrm{fm}^{-1}$. If the densities of the isolated slabs are less than half of the saturation density ϱ_0 (cases A and B), one gains energy by merging the two slabs, and thus $\mathscr{V}_R/A < 0$. In case C the densities of the isolated slabs are equal ϱ_0, and to merge the two slabs to a combined system of density $\varrho = 2\varrho_0$, we have to supply energy, and thus $\mathscr{V}_R > 0$.

The depth of the imaginary potential $\mathscr{V}_I/A$ increases with K_r, because more and more phase space allowed by the exclusion principle is available for the final states of the NN scattering. Whereas at large values of K_r (here $\bar{Q} \cong 1$) the absorption increases with ϱ, at small values of K_r it decreases with increasing ϱ. Namely, the dominant factor in determining the density dependence of $\mathscr{V}_I/A$ at small values of K_r is the reduction of $|\mathscr{V}_I|/A$ by the exclusion principle which is the more effective the higher the density.

Our way of calculating $\mathscr{V}/A$ may be regarded as an approximation to the work of Faessler and his collaborators [7–9]. These authors start with the Reid soft core NN potential [10], solve self-consistently the equations for the complex effective NN interaction (the Brueckner $\mathscr{K}$ matrix) for two slabs of NM, and use this interaction in calculating the complex energy density. We apply approximations which allow us to bypass the problem of determining $\mathscr{K}$ from a potential model. As it was shown in I, our results for $\mathscr{V}_R/A$ agree nicely with those of the Faessler group, especially if we replace our empirical NM parameters by the parameters of the "Reid soft core NM", i.e., the parameters calculated by the Faessler group with the Reid soft core potential.

The situation with $\mathscr{V}_I/A$, discussed in detail in I, is less satysfactory. In Fig. 4, we show

our results for $\mathscr{V}_I/A$ as functions of the total density ϱ for $K_r = 1, 2$, and $3\ \mathrm{fm}^{-1}$, together with the same "exact" results of the Faessler group, taken from the paper by Ohtsuka et al. [9]. In general, our absorptive potential is weaker than the "exact" one. Our frivolous model is expected to work best at high energies and low densities. The behaviour of the curves in Fig. 4 appears to agree with this expectation (except for the lowest densities considered, where the "exact" absorptive potential for $K_r = 2$, and $3\ \mathrm{fm}^{-1}$ becomes weaker

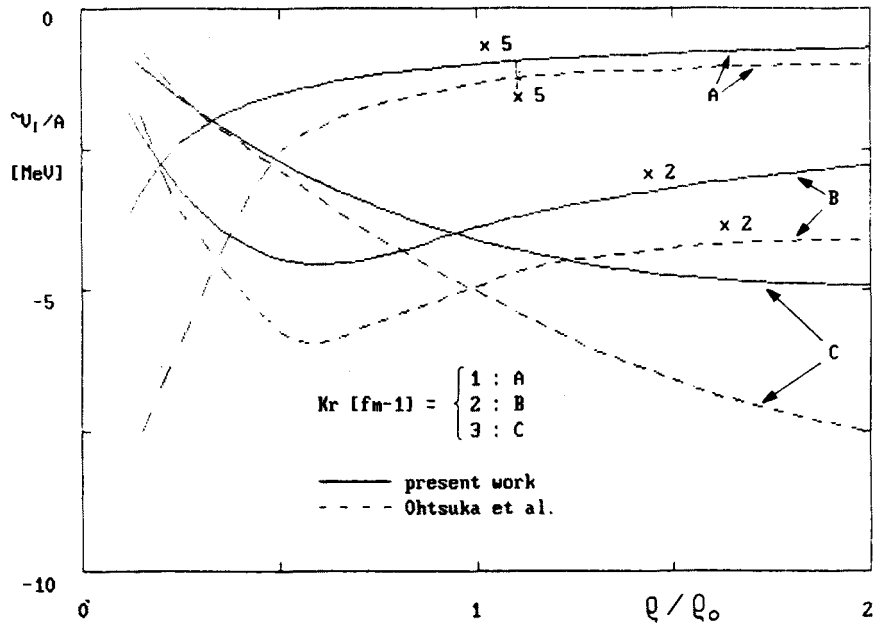

Fig. 4. $\mathscr{V}_I/A$ for two colliding slabs of NM of the same density as function of the ratio of the total density ϱ to the saturation density $\varrho_0 = 0.166\ \mathrm{fm}^{-3}$

than ours). Most serious is the discrepancy between our and the "exact" results for $K_r = 1\ \mathrm{fm}^{-1}$ and $0.1 \lesssim \varrho/\varrho_0 \lesssim 0.5$ (curve A).

The high density behaviour of our results is sensitive to the value of the effective mass $v = m^*/m$ (at low densities $v \cong 1$) which we assume not to depend on the momentum. In fact, with increasing momentum the effective mass is expected to increase. Taking it into account would increase the depth of our absorptive potential at larger values of K_r and higher densities, and thus reduce there the discrepancy with the "exact" results.

On the other hand, the convergence of the Brueckner theory deteriorates at high densities. Furthermore, the "exact" theory requires approximations for its execution, that may affect the reliability of the "exact" results in an uncontrolled way.

No doubt, the accuracy of our frivolous model of $\mathscr{V}_I$ should be investigated more carefully in spite of the fact that the model appears to work in the case of the nucleon--nucleus optical potential [11, 12].

5. *Inhomogeneity corrections*

Variations of the density, especially at the surface of the nuclar system where the effects of the finite range of the nuclear forces are important, lead to density gradient corrections to the energy density H. We take them into account in the same way as it was done by Brueckner et al. [2]. Namely, we add to the energy density the gradient correction

$$H_\nabla = \tau_\nabla + \pi_\nabla. \tag{5.1}$$

The gradient correction τ_∇ to the kinetic energy density, known as the Weizsäcker correction, is

$$\tau_\nabla = (\hbar^2/72m)\,(\nabla\varrho)^2/\varrho. \tag{5.2}$$

(Notice the additional factor 1/9 compared to the original form of the Weizsäcker correction.)

For the gradient correction π_∇ to the potential density, we use the form

$$\pi_\nabla = \eta(\nabla\varrho)^2, \tag{5.3}$$

and treat η as a free parameter which we fix by requiring that the intrinsic nuclear energies $\mathscr{E}_{\text{in}}$ (plus the Coulomb energies) calculated for ^{16}O and ^{40}Ca agree with the experimental energies.

We calculate $\mathscr{E}_{\text{in}}$ for ^{16}O and ^{40}Ca according to the expression

$$\mathscr{E}_{\text{in}} = \int dr\{f(\tilde{\varrho})\tilde{\varrho} + (\hbar^2/72m)\,(\nabla\tilde{\varrho})^2/\tilde{\varrho} + \eta(\nabla\tilde{\varrho})^2\}, \tag{5.4}$$

where $\tilde{\varrho}$ is the density in ^{16}O and ^{40}Ca respectively.

For $\tilde{\varrho}$ we use the density distributions determined by electron scattering [13]. For ^{16}O we use the modified harmonic oscillator distribution

$$\tilde{\varrho}(^{16}\text{O}; r) = \tilde{\varrho}_0[1+\alpha(r/c)^2]\exp\{-(r/c)^2\}, \tag{5.5}$$

with $\alpha = 1.544$, $c = 1.833$ fm ($\tilde{\varrho}_0 = 0.1407$ fm^{-3}, $\sqrt{\langle r^2\rangle} = 2.718$ fm), and for ^{40}Ca the three-parameter Fermi distribution

$$\tilde{\varrho}(^{40}\text{Ca}; r) = \tilde{\varrho}_0[1+w(r/c)^2]/[1+\exp\{(r-c)/z\}], \tag{5.6}$$

with $w = -0.161$, $c = 3.766$ fm, $z = 0.586$ fm ($\tilde{\varrho}_0 = 0.1698$ fm^{-3}, $\sqrt{\langle r^2\rangle} = 3.482$ fm). For $r/c > 1/\sqrt{-w}$, we put $\tilde{\varrho} = 0$. These densities were used in drawing Fig. 1 in which $\varrho_1 = \tilde{\varrho}(^{40}\text{Ca})$, $\varrho_2 = \tilde{\varrho}(^{16}\text{O})$, and $\varrho = \varrho_1 + \varrho_2$.

For the Coulomb energy of ^{16}O and ^{40}Ca, we use the expression

$$E_{\text{Coul}} = 3Z^2e^2/5R_{\text{C}}, \tag{5.7}$$

where $R_{\text{C}} = [5\langle r^2\rangle/3]^{1/2}$ [$R_{\text{C}}(^{16}\text{O}) = 3.51$ fm, $R_{\text{C}}(^{40}\text{Ca}) = 4.49$ fm]. Expression (5.7) represents the Coulomb energy of a uniform charge distribution with the same r.m.s. as $\tilde{\varrho}$ (following [14], we use Z^2 instead $Z(Z-1)$, and neglect the exchange part).

TABLE I

Ground state energies (MeV) for ^{16}O and ^{40}Ca

	^{16}O	^{40}Ca
Kinetic energy	217.4	604.7
Weizsäcker term	11.9	19.2
Potential energy	−387.2	−1071.2
$\eta(\nabla\varrho)^2$ term[a]	16.1	28.5
Coulomb energy	15.8	76.9
Total	−126.0	−341.9
Experimental	−127.6	−342.1

[a] $\eta = 22$ MeV fm^5.

Table I shows the energies obtained for ^{16}O and ^{40}Ca with $\eta = 22$ MeV fm^5. The nice agreement with the experimental energies of both nuclei obtained with the empirical densities and with the same value of η indicates that the form of our energy density is basically correct. This value of η will be used in all our calculations.

6. *Calculational procedure*

To calculate the optical potential $\mathscr{V}$ for the scattering of nucleus 2 (projectile) on nucleus 1 (target), we apply the local density approximation (plus inhomogeneity corrections) and the frozen density model. This means that locally (at each point $\boldsymbol{r}$ — see Fig. 1) the system is approximated by two slabs of NM with the total density $\varrho(\boldsymbol{r})$ given by Eq. (3.1), and with the two-sphere momentum distribution of Fig. 2.

As in Sect. 2.1, we calculate the energy density H in the cm frame of the two slabs. Now, the cm frame depends on $\boldsymbol{r}$ (is local). Thus before calculating the energy $\mathscr{E}$, we go over to the rest frame of slab 1, which we call the "laboratory" (lab) frame. This frame — in our frozen density approximation — coincides with the rest frame of nucleus 1 and does not depend on $\boldsymbol{r}$. [Of course, it depends on R; at $R = \infty$ it coincides with the laboratory (LAB) frame of nuclei 1 and 2 with nucleus 1 being the target.]

In the lab frame, we have

$$\mathscr{E}_{\mathrm{lab}}(K_{\mathrm{REL}}, R) = \int d\boldsymbol{r}\{H_{\mathrm{lab}}(K_{\mathrm{REL}}, R; \boldsymbol{r}) + H_{\mathrm{V}}\} \tag{6.1}$$

where

$$H_{\mathrm{lab}} = H + (\hbar^2/2m)k_{\mathrm{G}}^2\varrho. \tag{6.2}$$

By $\boldsymbol{k}_{\mathrm{G}}$ we denote the momentum per nucleon in the local two slabs of NM in the lab system:

$$\boldsymbol{k}_{\mathrm{G}} = \int_{\mathrm{F}} d\boldsymbol{k}'_{\mathrm{N}}\boldsymbol{k}'_{\mathrm{N}}/V_{\mathrm{F}}, \tag{6.3}$$

where $\boldsymbol{k}'_{\mathrm{N}} = \boldsymbol{k}_{\mathrm{N}} + \boldsymbol{k}_{\mathrm{G}}$ is the nucleon momentum in the lab frame. The integration in (6.3) over momenta inside the Fermi surface F may be easily performed, which leads to a simple expression for $\boldsymbol{k}_{\mathrm{G}}$ in terms of $\boldsymbol{K}_{\mathrm{r}}$, k_{F1} and k_{F2} [see Eq. (3.1) of I].

To determine $\mathscr{V}_R$, we use Eq. (2.1), and the relation

$$\mathscr{E}_{lab} = \mathscr{E}_{CM} + (\hbar K_2)^2/2(M_1 + M_2), \tag{6.4}$$

where $K_2 = (M_2/\mu)K_{REL}$ is the momentum of nucleus 2 in the lab frame. We get:

$$\mathscr{V}_R(E, R) = \mathscr{E}_{lab}(K_{REL}, R) - (\hbar M_2 K_{REL}/\mu)^2/2M_2 - \mathscr{E}_{in}(1) - \mathscr{E}_{in}(2). \tag{6.5}$$

For a given CM energy E, we know only $K_{REL}(\infty) = (2\mu E)^{1/2}/\hbar$, whereas expression (6.5) for $\mathscr{V}_R(E, R)$ depends on $K_{REL} = K_{REL}(R)$, connected with $K_{REL}(\infty)$ by energy conservation Eq. (2.3) which in turn contains $\mathscr{V}_R(E, R)$. We solve this problem by iteration which we start by calculating $\mathscr{V}_R^{(0)}$ with the help of expression (6.5) with $K_{REL} = K_{REL}(\infty)$. In the next step, we calculate $\mathscr{V}_{REL}^{(1)}$ by applying expression (6.5) with $K_{REL} = K_{REL}^{(1)}(R)$, obtained from Eq. (2.3) with $\mathscr{V}_R = \mathscr{V}_R^{(0)}$. After a few steps, we obtain $\mathscr{V}_R^{(i)} = \mathscr{V}_R^{(i-1)} = \mathscr{V}_R$.

To calculate $\mathscr{V}_I$, we apply expressions (2.15) and (2.22). Notice that expression (2.22) for the absorptive potential density v_I contains the local two-sphere momentum distribution n of Fig. 2, which depends on $K_{REL}(R)$. This presents no problem, because after determining $\mathscr{V}_R$, we know $K_{REL}(R)$ from energy conservation Eq. (2.3).

The connection between E_{LAB}/A_P (the kinetic energy of the projectile nucleus per projectile nucleon in the LAB system) and $K_r(\infty)$ [in fm^{-1}] is:

$$E_{LAB}/A_p = (\hbar^2/2m)K_r(\infty)^2 = 20.7\ K_r(\infty)^2\ \text{MeV}. \tag{6.6}$$

For the r-integration in (6.1) and (2.15), we use cylindrical coordinates with the z-axis along $\boldsymbol{R}$. We assume that $\boldsymbol{K}_r$ is parallel to $\boldsymbol{R}$, which reduces the r-integration to a twofold integration. Whereas we have analytical expressions for H, expression (2.22) for v_I involves integrations over $\boldsymbol{k}_1$ and $\boldsymbol{k}_2$. These integrations, in cylindrical coordinates along $\boldsymbol{K}_r$, lead to a five-dimensional integration. All the integrations have been performed by means of the Gauss formula.

7. Results for ^{16}O and ^{40}Ca and discussion

In all our calculations, we use the density distributions of ^{16}O and ^{40}Ca described in Sect. 5, and the NM parameters and the parametrization of the NN cross section σ described in Sect. 6. The inhomogeneity corrections described in Sect. 5 are included in our calculations.

To obtain $\mathscr{V}_C(R)$ we approximate charge distributions in nuclei 1 and 2 by equivalent uniform charge distributions (see Sect. 5) and calculate $\mathscr{V}_C(R)$ as the Coulomb interaction between these two uniform charge distributions. Results obtained for $\mathscr{V}_C(R)$ are shown in Fig. 5.

The role of the dependence of K_r on R is illustrated in Fig. 6 in the case of the potential $\mathscr{V}$ between two ^{16}O nuclei at $K_r(\infty) = 1$ fm^{-1}. Results for $\mathscr{V}_R$ and $\mathscr{V}_I$ obtained with $K_r = K_r(\infty)$ are drawn as broken curves, whereas those obtained with $K_r = K_r(R)$ [connected with $K_r(\infty)$ by Eq. (2.3)] as solid curves. Both curves for $\mathscr{V}_R$ represent an attractive potential. Also the total potential $\mathscr{V}_{R,tot} = \mathscr{V}_R + \mathscr{V}_C$ (see Fig. 5) is attractive [only for $R \gtrsim 6$ fm

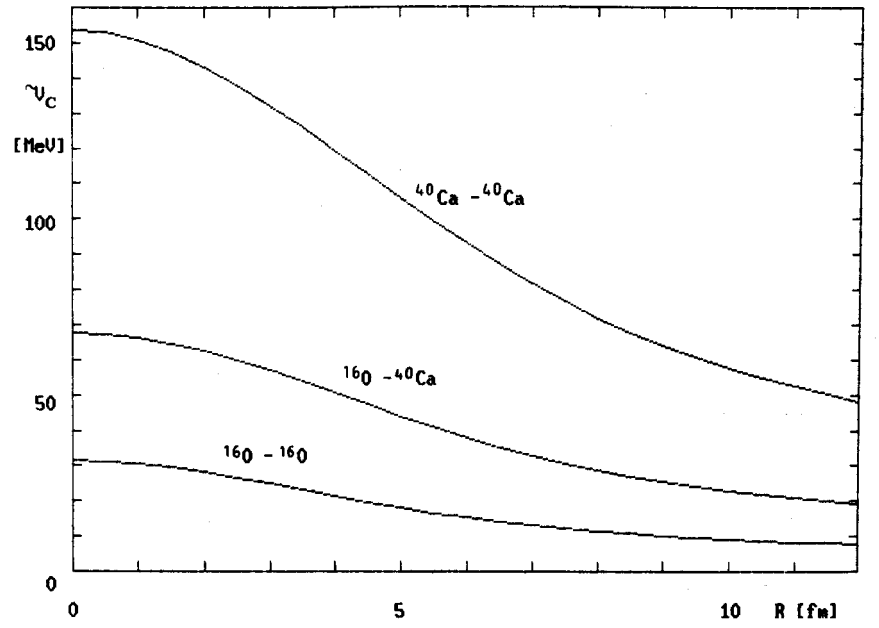

Fig. 5. Coulomb potential $\mathscr{V}_C(R)$ between heavy ions

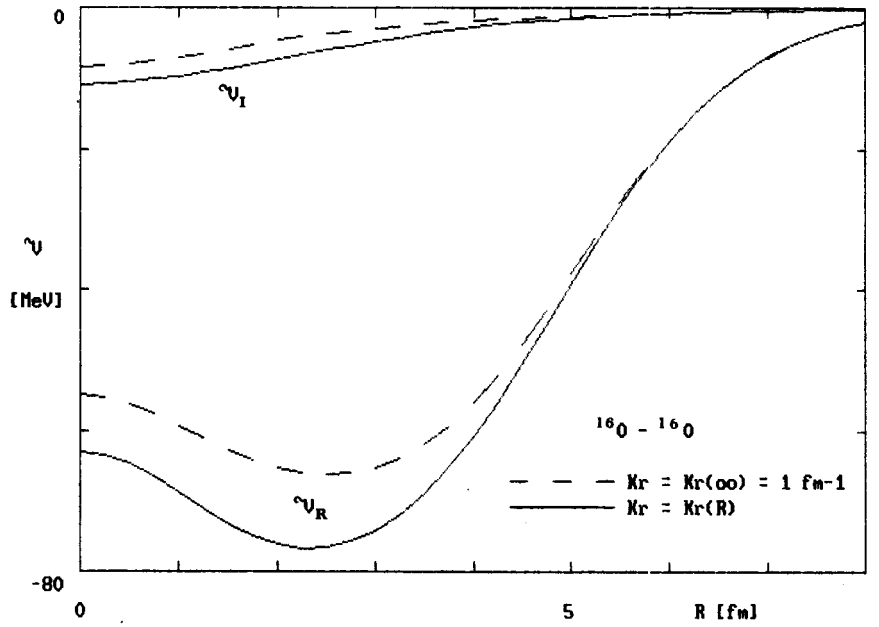

Fig. 6. $\mathscr{V}_R$ and $\mathscr{V}_I$ for ^{16}O–^{16}O at $K_r(\infty) = 1$ fm^{-1} calculated with and without the R dependence of K_r

is $\mathcal{V}_{R,tot}$ repulsive but small, and the change in $\mathcal{V}_R$ introduced by the dependence of K_r on R is here very small] and thus we have $K_r(R) > K_r(\infty)$ [see Eq. (2.3)]. Looking at Fig. 3, we notice that $\mathcal{V}_R$ decreases with increasing K_r at $K_r = 1\ \mathrm{fm}^{-1}$ (we are here below the "window" at $K_r \cong 1.5\ \mathrm{fm}^{-1}$). Consequently $\mathcal{V}_R(K_r(R), R) < \mathcal{V}_R(K_r(\infty), R)$ as is seen in Fig. 6.

Situations different from that shown in Fig. 6 may also occur. For an attractive $\mathcal{V}_{R,tot}$ at K_r above the "window", we have $\mathcal{V}_R(K_r(R), R) > \mathcal{V}_R(K_r(\infty), R)$. For a repulsive $\mathcal{V}_{R,tot}$ the situation is reversed: $\mathcal{V}_R(K_r(R), R) > \mathcal{V}_R(K_r(\infty), R)$ at K_r below the "window" ($K_r \lesssim 1.5\ \mathrm{fm}^{-1}$), and $\mathcal{V}_R(K_r(R), R) < \mathcal{V}_R(K_r(\infty), R)$ at K_r above the "window" ($K_r \gtrsim 1.5\ \mathrm{fm}^{-1}$).

The behaviour of $\mathcal{V}_I$ is simpler, since $\mathcal{V}_I$ decreases monotonically with increasing K_r. Consequently, $\mathcal{V}_I(K_r(R), R) < \mathcal{V}_I(K_r(\infty), R)$ for an attractive $\mathcal{V}_{R,tot}$ (the situation in Fig. 6), and $\mathcal{V}_I(K_r(R), R) > \mathcal{V}_I(K_r(\infty), R)$ for a repulsive $\mathcal{V}_{R,tot}$.

The dependence of K_r on R, Eq. (2.3), has been considered also by Müller [15], and partly [with the Coulomb potential neglected in Eq. (2.3)] by Ohtsuka et al. [9].

The importance of the inhomogeneity correction is illustrated in Fig. 7. To explain the R dependence of this correction, let us start from a large distance R, at which the two ^{16}O nuclei are spatially separated. When we decrease R, the two nuclei begin overlapping and the surface of the combined system (originally equal twice the surface of ^{16}O) decreases. Since it is the surface region in which $(\nabla\varrho)^2 \neq 0$, the (positive) inhomogeneity correction to the energy of the combined system decreases, and thus the inhomogeneity correction to $\mathcal{V}_R$ is negative (attractive). When the two nuclei overlap completely ($R \to 0$), the surface of the combined system becomes minimal (equal to the surface of ^{16}O). Here, however,

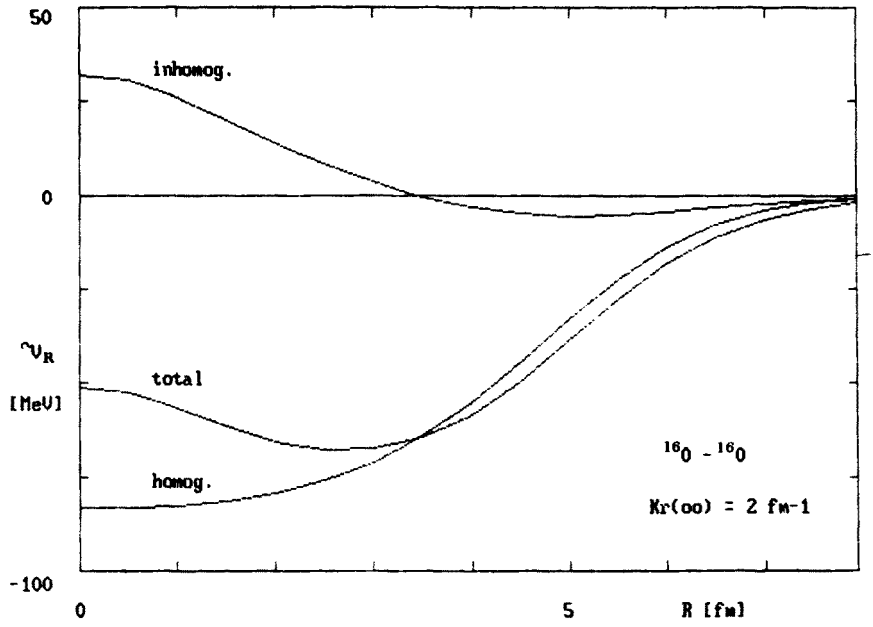

Fig. 7. Contribution of the inhomogeneity correction to $\mathcal{V}_R$ for ^{16}O–^{16}O at $K_r(\infty) = 2\ \mathrm{fm}^{-1}$

$\varrho(r) = 2\tilde{\varrho}(^{16}\mathrm{O}; r)$, and $(\nabla\varrho)^2 = 4(\nabla\tilde{\varrho})^2$. Thus the increase in $(\nabla\varrho)^2$ by a factor 4 compared to $(\nabla\tilde{\varrho})^2$ becomes more important than the decrease in the surface (by a factor 2 compared to the surface of two separated ^{16}O nuclei). Consequently, the inhomogeneity contribution to $\mathscr{V}_R$ at small distances R is positive (repulsive). [The above reasoning applies to the inhomogeneity correction $\pi_\nabla \sim (\nabla\varrho)^2$. A similar reasoning applied to the Weizsäcker term $\tau_\nabla \sim (\nabla\varrho)^2/\varrho$ shows that its contribution to $\mathscr{V}_R$ vanishes at $R = 0$, and is attractive for $R \neq 0$.]

We use the frozen density model, and a rough criterion for its applicability is that E_{LAB}/A_P should be larger than the intrinsic kinetic energy per nucleon in the colliding nuclei, i.e., about 30 MeV. This implies the condition $K_r(\infty) \gtrsim 1.2\,\mathrm{fm}^{-1}$ [see Eq. (6.6)]. On the other hand, an upper limit on K_r is imposed by our use of the nonrelativistic theory: for $K_r(\infty) = 3.4\,\mathrm{fm}^{-1}$, we already have $E_{LAB}/A_P \cong \frac{1}{4}mc^2$.

Our final results for $\mathscr{V}(R)$ for $K_r(\infty) = 1$, 1.5, 2, and 2.5 fm^{-1} (i.e., for $E_{LAB}/A_P = 21$, 47, 83, and 130 MeV) are shown in Fig. 8 for ^{16}O–^{16}O, in Fig. 9 for ^{16}O–^{40}Ca, and in Fig. 10 for ^{40}Ca–^{40}Ca.

The most striking feature of our results is the strong dependence of both $\mathscr{V}_R$ and $\mathscr{V}_I$ on $K_r(\infty)$, i.e. on the energy E. It reflects the dependence of $\mathscr{V}_R/A$ and $\mathscr{V}_I/A$ on K_r for two slabs of NM, discussed in Sect. 4. The increase in $|\mathscr{V}_I|/A$ with increasing K_r (see Fig. 3) leads to the fast increase in the depth of $\mathscr{V}_I$ with increasing $K_r(\infty)$ seen in Figs 8–10. The fact that $\mathscr{V}_R$ in Figs 8–10 is most attractive for $K_r(\infty) = 1.5\,\mathrm{fm}^{-1}$ is caused by the "window" of a minimum in $\mathscr{V}_R/A$ at $K_r \cong 1.5\,\mathrm{fm}^{-1}$ in Fig. 3.

At small distances R the potential $\mathscr{V}_R(R)$ is less atractive, and becomes repulsive

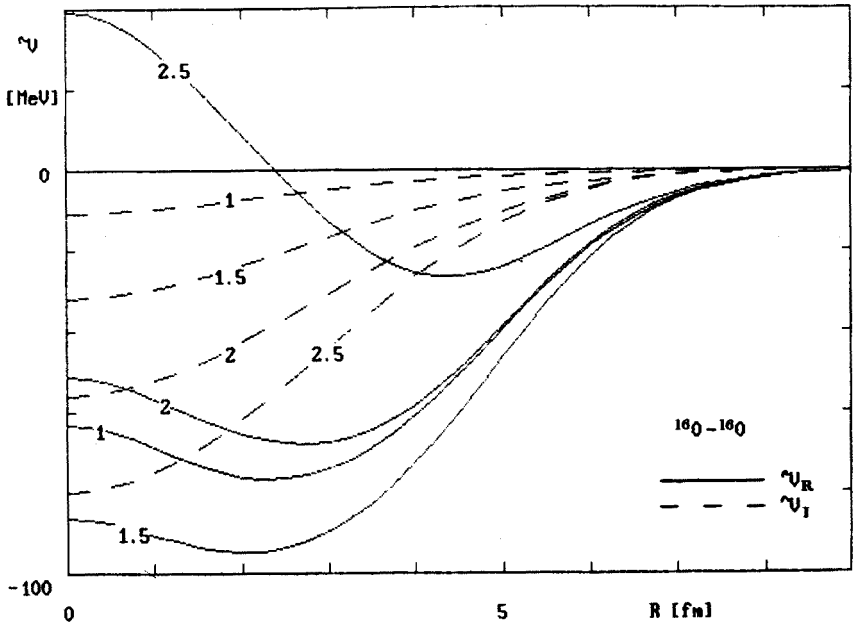

Fig. 8. $\mathscr{V}_R$ and $\mathscr{V}_I$ for ^{16}O–^{16}O at the indicated values (in fm^{-1}) of K_r

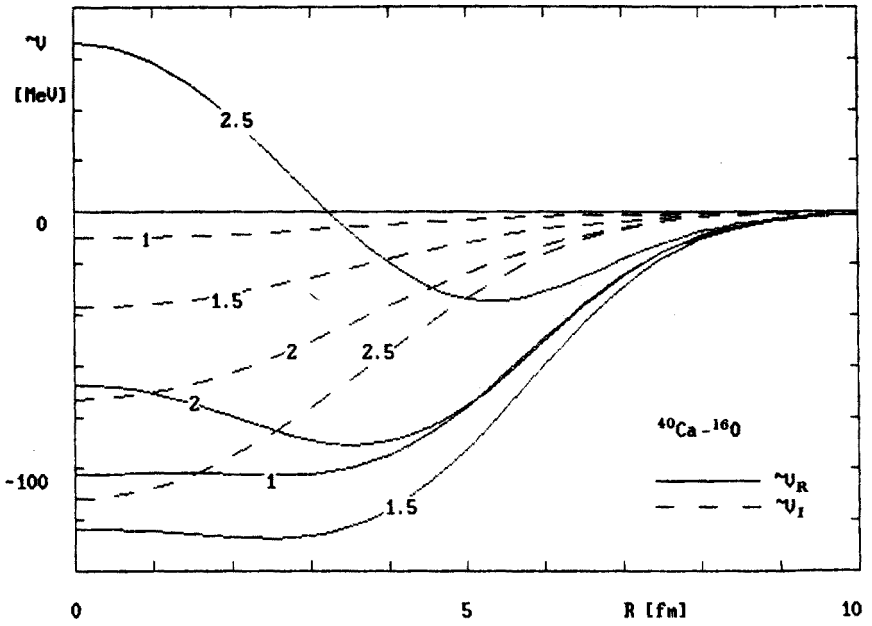

Fig. 9. $\tilde{V}_R$ and $\tilde{V}_I$ for ^{40}Ca–^{16}O at the indicated values (in fm^{-1}) of K_r

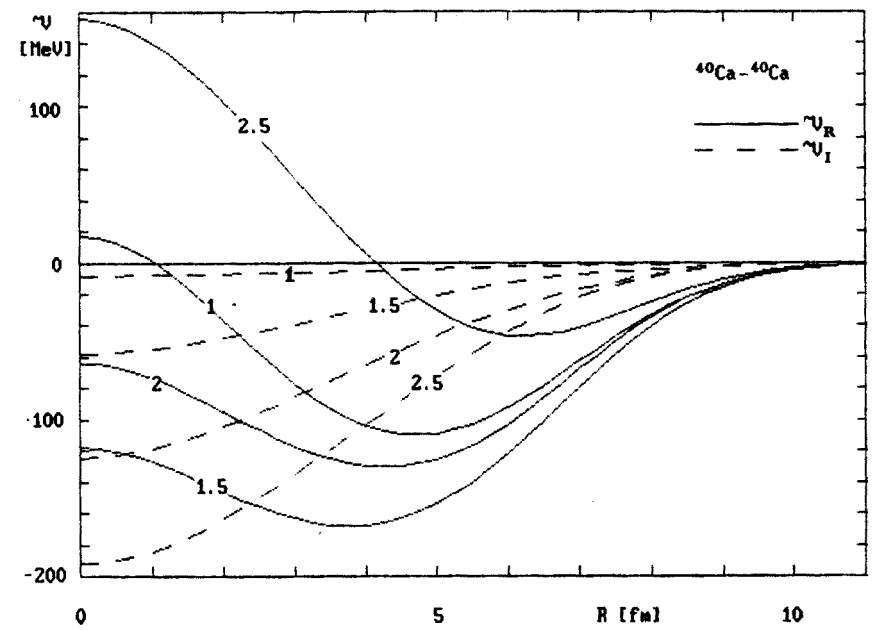

Fig. 10. $\tilde{V}_R$ and $\tilde{V}_I$ for ^{40}Ca-^{40}Ca at the indicated values (in fm^{-1}) of K_r

at large values of $K_r(\infty)$ and also at small values of $K_r(\infty)$ [see ^{40}Ca–^{40}Ca at $K_r(\infty) = 1$ fm^{-1}]. This repulsion at small distances R is caused by the following factors:

— At $R \cong 0$ a substantial part of the combined system has the density $\varrho > \varrho_0$, which gives a repulsive contribution to $\mathscr{V}_R$.

— In the region where $k_{F10}(r)+k_{F20}(r) = (3\pi^2/2)^{1/3}\{\varrho_1(r)^{1/3}+\varrho_2(|r-R|)^{1/3}\} > K_r$, the increase in the kinetic energy caused by the Pauli blocking gives a repulsive contribution to $\mathscr{V}_R$. With increasing K_r the region shrinks and the contribution decreases. It disappears completely for $K_r \gtrsim k_{F10}(0)+k_{F20}(0) \cong 2(3\pi^2\varrho_0/2)^{1/3} = 2.7$ fm^{-1}.

— The potential energy contribution to $\mathscr{V}_R$ increases (algebraically) with increasing K_r. It may be traced back to the short range NN repulsion.

— Our inhomogeneity correction is repulsive at $R \cong 0$ (it does not depend on K_r).

The absorptive potential $\mathscr{V}_I$ is concentrated at small distances R. Its range is short compared with the range of $\mathscr{V}_R$. It should be stressed that our absorptive potential arises entirely from the two-body mechanism of incoherent NN collisions. However, the damping of the elastic channel in the heavy-ion scattering may arise also from coherent excitations of collective states. These genuine surface effects, disregarded in our NM approach, are expected to increase the range of the imaginary potential [16].

Our results for $\mathscr{V}_R(R)$ and $\mathscr{V}_I(R)$ for the ^{16}O–^{16}O system at $K_r(\infty) = 1$ fm^{-1} are compared in Fig. 11 with the same results of Ohtsuka et al. [9], calculated in the frozen density approximation with the "exact" energy density H obtained by solving the $\mathscr{K}$ matrix equations with the Reid soft core NN potential.

The agreement of the results for $\mathscr{V}_R(R)$ is quite satisfactory, in spite of some differences

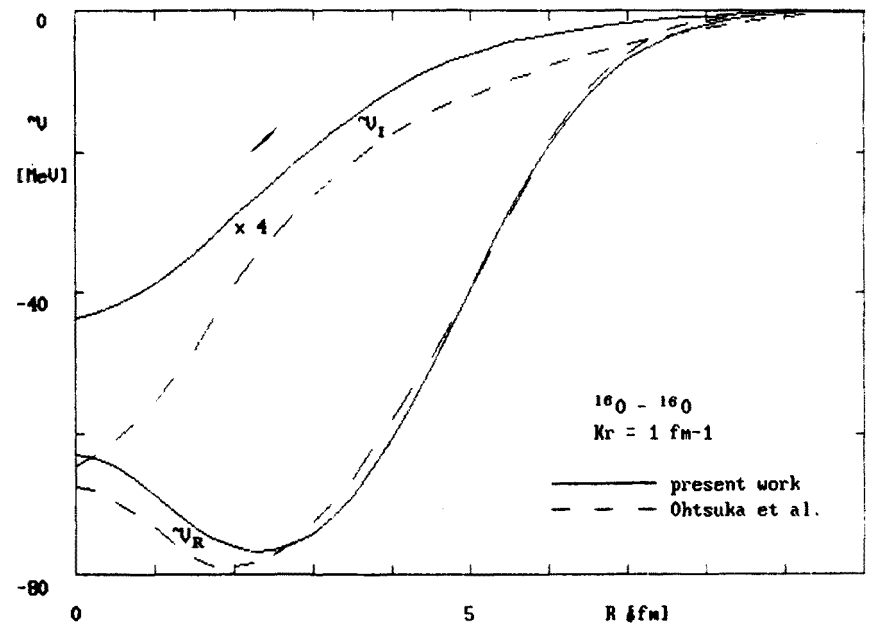

Fig. 11. Present result for $\mathscr{V}_R(R)$ for ^{16}O–^{16}O at $K_r = 1$ fm^{-1} compared with the result of Ohtsuka et al. [9]

in the two calculations. Ohtsuka et al. have an equation of state of NM (calculated with the Reid soft core potential) softer than ours, which however is balanced by their neglect of the dependence of K_r on R (see Fig. 6). They do not consider τ_∇ and instead of our expression (5.1), they use the inhomogeneity correction $H_\nabla = \pi_\nabla$ with a correspondingly bigger value of η. Furthermore, their density $\tilde{\varrho}(^{16}\mathrm{O}; r)$ differs from ours. Also their prescription to avoid the double occupancy when the two Fermi spheres overlap [17], differs (for $k_{\mathrm{F}10} \neq k_{\mathrm{F}20}$) from our prescription (3.5).

On the other hand, our absorptive potential $\mathscr{V}_\mathrm{I}(R)$ is much weaker than that calculated by Ohtsuka et al. This discrepancy [which is actually diminished by our use of $K_r = K_r(R)$, whereas Ohtsuka et al. use $K_r \equiv K_r(\infty)$] simply reflects the similar discrepancy in $\mathscr{V}_\mathrm{I}/A$ in Fig. 4, which is particularly big for $K_r = 1\ \mathrm{fm}^{-1}$. Looking at Fig. 4, one would expect the discrepancy in $\mathscr{V}_\mathrm{I}(R)$ to become smaller at higher values of $K_r(\infty)$, where in fact also the frozen density approximation is more reliable.

8. *Conclusion*

Our method of calculating $\mathscr{V}_\mathrm{R}(R)$ is principally identical — except for one essential difference — with the energy density formalism, applied by Brueckner et al. [2]. (A newer version of Brueckner's method is the work of Ngô et al. [18].) It is based on definition (2.1) of $\mathscr{V}_\mathrm{R}$ and on the local density approximation, Eq. (2.4), with the energy density equal to that of the local NM. The essential difference is that whereas in the Brueckner method the system of colliding nuclei is represented locally by a piece of normal NM (with the corresponding energy density H_0), in the present work it is represented locally by two pieces of NM flowing through each other with the relative velocity K_r/m (with the corresponding energy density H). In other words, we take into account that the local momentum distribution n in the system of colliding nuclei differs from the distribution n_0 in normal NM. The dependence of our energy density H on K_r leads to the strong energy dependence of the resulting $\mathscr{V}_\mathrm{R}(R)$, whereas the potential $\mathscr{V}_\mathrm{R}(R)$ calculated with H_0 does not depend on energy.

For the local momentum distribution n, we use the two Fermi sphere model, used before by Saloner et al. [19–20], Beck et al. [5], Müller [15], Peng et al. [21–22], and by the Faessler group [7–9, 16–17, 23]. Whereas in all these papers (except for [21–22]) the "exact" energy density H was calculated with the Brueckner $\mathscr{K}$ matrix, determined by solving the $\mathscr{K}$ matrix equations with a given NN interaction, we use for H_0 a simple form, Eqs. (2.8) and (2.13), fitted to known properties of NM, and use relation (2.9) to determine the difference H-H_0. Our results for $\mathscr{V}_\mathrm{R}(R)$ are in a reasonable agreement with the results of the most extensive "exact" calculations of the Faessler group.

For the imaginary potential $\mathscr{V}_\mathrm{I}$, we use the frivolous model (which may be linked to the "exact" theory through the optical theorem — see I). In this way we express $\mathscr{V}_\mathrm{I}$ directly through the NN cross section. This approach was applied before in [20] (with an incomplete treatment of the Pauli blocking) and in [21–22] (for calculating the heavy-ion total and reaction cross section — without taking into account dispersive effects). Our resulting $\mathscr{V}_\mathrm{I}$ appears too weak compared with the "exact" results of the Faessler group.

The strong point of our approach is that the input for calculating $\mathscr{V}$ consists of empirical parameters of NM and the NN cross section. Furthermore, the calculation is straightforward and its execution does not require any approximations.

The following weak points of our procedure should be mentioned.

— To determine H-H_0, we use relation (2.9) valid for small values of K_r. On the other hand, the frozen density model favours large values of K_r.

— To construct the local momentum distribution when the two Fermi spheres overlap, we use an ad hoc prescription, Eqs. (3.5) and (3.6).

— In calculating $\mathscr{V}_1$, we apply the frivolous model whose accuracy is hard to assess.

All these points require further investigation.

It is the pleasure of the author to acknowledge several discussions with H. S. Köhler.

REFERENCES

[1] J. Dąbrowski, H. S. Köhler, *Nucl. Phys.* — submitted.
[2] K. A. Brueckner, J. R. Buchler, S. Jorna, R. L. Lombard, *Phys. Rev.* **171**, 1188 (1968).
[3] A. Bohr, B. R. Mottelson, *Nucler Structure*, Vol. I, W. A. Benjamin Inc., 1969.
[4] B. Friedman, V. R. Pandharipande, *Phys. Lett.* **100B**, 205 (1981).
[5] F. Beck, K.-H. Müller, H. S. Köhler, *Phys. Rev. Lett.* **40**, 837 (1978).
[6] N. R. Metropolis et al., *Phys. Rev.* **110**, 204 (1958).
[7] T. Izumoto, S. Krewald, A. Faessler, *Nucl. Phys.* **A341**, 319 (1980).
[8] T. Izumoto, S. Krewald, A. Faessler, *Nucl. Phys.* **A357**, 471 (1981).
[9] N. Ohtsuka, R. Linden, A. Faessler, F. B. Malik, *Nucl. Phys.* **A465**, 550 (1987).
[10] R. V. Reid, *Ann. Phys.* (N.Y.) **50**, 411 (1968).
[11] H. S. Köhler, *Nucl. Phys.* **A415**, 37 (1984).
[12] J. Dąbrowski, W. Piechocki, *Acta Phys. Pol.* **B16**, 1095 (1985).
[13] C. W. de Jager, H. de Vries, C. de Vries, *At. Nucl. Data Tables* **14**, 479 (1974).
[14] D. C. Peaslee, *Phys. Rev.* **95**, 717 (1954).
[15] R.-H. Müller, Dissertation, Technische Hochschule Darmstadt, April 1979, D17; *Z. Phys.* **A295**, 79 (1980).
[16] S. B. Khadkikar, L. Rikus, A. Faessler, R. Sartor, *Nucl. Phys.* **A369**, 495 (1981).
[17] M. Trefz, A. Faessler, W. H. Dickhoff, *Nucl. Phys.* **A443**, 499 (1985).
[18] C. Ngô, B. Tamain, M. Beiner, R. J. Lombard, D. Mass, H. H. Deubler, *Nucl. Phys.* **A252**, 237 (1975).
[19] D. A. Saloner, C. Toepffer, *Nucl. Phys.* **A283**, 108 (1977).
[20] D. A. Saloner, C. Toepffer, B. Fink, *Nucl. Phys.* **A283**, 131 (1977).
[21] J. C. Peng, R. M. De Vries, N. J. Giacomo, *Phys. Lett.* **98B**, 244 (1981).
[22] N. J. Giacomo, J. C. Peng, R. M. De Vries, *Phys. Lett.* **101B**, 383 (1981).
[23] N. Ohtsuka, A. Faessler, *Z. Phys.* **A329**, 89 (1988).